Three-Dimensional Plasmon Rulers

Na Liu, *et al.*

Science **332**, 1407 (2011);
DOI: 10.1126/science.1199958

Three-Dimensional Plasmon Rulers

Na Liu,[1]* Mario Hentschel,[2] Thomas Weiss,[2,3] A. Paul Alivisatos,[1] Harald Giessen[2]

Plasmon rulers can be used to determine nanoscale distances within chemical or biological species. They are based on the spectral shift of the scattering spectrum when two plasmonic nanoparticles approach one another. However, the one-dimensionality of current plasmon rulers hampers the comprehensive understanding of many intriguing processes in soft matter, which take place in three dimensions. We demonstrated a three-dimensional plasmon ruler that is based on coupled plasmonic oligomers in combination with high-resolution plasmon spectroscopy. This enables retrieval of the complete spatial configuration of complex macromolecular and biological processes as well as their dynamic evolution.

When two metallic nanoparticles are in close proximity, their plasmon resonances couple with each other and generate a light-scattering spectrum that depends strongly on the interparticle distance. This effect has been used to create plasmon rulers, (*1*), which can be used to measure nanoscale distances in one dimension. Plasmon rulers based on sensitive colorimetric schemes have been developed for monitoring DNA hybridization (*2*) and biological activities in living cells (*3*). Compared to molecular rulers based on dye-pair fluorescence resonance energy transfer (*4*), plasmon rulers offer exceptional photostability and brightness because of the use of noble metal nanoparticles. Beyond dimers, multiple nanoparticles can be placed in proximity to each other (*5*–*7*). In the resulting assemblies, plasmonic coupling would lead to light-scattering spectra that are sensitive to a complete set of three-dimensional (3D) motions. Such a 3D ruler would have great impact in many fields of biology and soft materials science by providing a complete picture of time-dependent nanoscale motions and rearrangements. However, typical dipolar plasmon resonances are broad because of radiative damping (*8*), and as a result the simple coupling between multiple particles produces indistinct spectra that are not readily converted into distances. We used high-resolution plasmon spectroscopy in combination with plasmon-induced transparency and higher-order resonances to overcome these limitations, and we demonstrated a 3D plasmon ruler. This offers a blueprint to optically determine the structural dynamics of single 3D entities. Commonly, techniques such as nuclear magnetic resonance and x-ray diffraction are used to determine 3D structural information. These techniques generally require a large amount of analyte to obtain good signals, hampering applications at the single-entity level. Additionally, x-ray diffraction does not work in situ or in vivo and involves complicated sample crystallization processes.

The key development reported here is the ability to create sharp spectral features in the otherwise broad resonance profile of plasmon-coupled nanostructures by using interactions between quadrupolar and dipolar modes (*9*–*11*). Such interactions can occur when multiple plasmonic particles are appropriately placed in close proximity to each other. The elementary building blocks of this 3D ruler are five gold nanorods of individually controlled length and orientation (Fig. 1A). The dipolar resonance of a single nanorod (for instance, the one shown in red in Fig. 1A) can be strongly driven by incident electromagnetic radiation. The optical response from such a nanorod is broad, due to strong radiative coupling to light. When two nanorods are placed parallel to each other (as in the pairs of yellow and green nanorods in Fig. 1A), under certain circumstances quadrupolar coupling to the incident radiation is possible, giving rise to a much sharper resonance due to significant suppression of radiative damping (*10*–*13*). In our 3D plasmon ruler, a single nanorod is placed in close proximity to two pairs of parallel nanorods (Fig. 1A). The strong coupling between the single nanorod and the two nanorod pairs allows for the excitation of two sharp quadrupolar resonances in the broad dipolar resonance profile, which in turn enables high-resolution plasmon spectroscopy. We could term this "double plasmon-induced transparency." Any conformational change of this 3D plasmonic structure produces readily observable changes in the spectrum.

As a proof of concept, we fabricated a series of samples using high-precision electron beam lithography and layer-by-layer stacking nanotechniques (*14*). The whole metallic structure was embedded in a dielectric medium (PC403) and resided on a glass substrate. The middle nanorod (in red, Fig. 1) is perpendicularly stacked between two parallel rod pairs (in yellow and green). The lengths of the top yellow and bottom green rod pairs are L_1 and L_2, respectively. The middle rod is displaced from the symmetry axis of the bottom green rod pair by S. The vertical distance between the red rod and the yellow rod pair is H_1; that between the red rod and the green rod pair is H_2. Electron micrographs of the fabricated structures were obtained by field-emission scanning

[1]Department of Chemistry, University of California, Berkeley, and Materials Sciences Division, Lawrence Berkeley National Laboratory, Berkeley, CA 94720, USA. [2]4. Physikalisches Institut and Research Center Scope, Universität Stuttgart, D-70569 Stuttgart, Germany. [3]LASMEA, University Blaise Pascal, 24 Avenue des Landais, 63177 Aubière Cedex, France.

*To whom the correspondence should be addressed. E-mail: nliu@lbl.gov

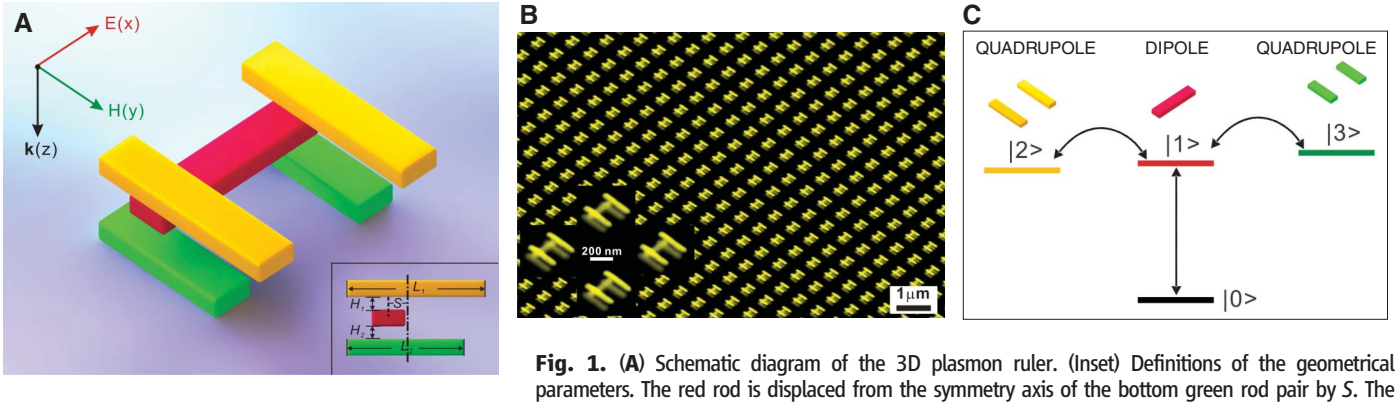

Fig. 1. (**A**) Schematic diagram of the 3D plasmon ruler. (Inset) Definitions of the geometrical parameters. The red rod is displaced from the symmetry axis of the bottom green rod pair by S. The lengths of the top yellow and bottom green rods are L_1 and L_2, respectively. The vertical distance between the red rod and the yellow rod pair is H_1, and that between the red rod and the green rod pair is H_2. E, electric field; H, magnetic field; k, direction of light propagation. (**B**) SEM image of a typical sample fabricated by electron beam lithography. The scale bar is 200 nm. The structure is on a glass substrate. The gold rods are embedded in a photopolymer (PC403), which serves as a dielectric spacer. All the gold rods have the same thickness and width, which are 40 and 80 nm, respectively. $S = 40$ nm, $H_1 = H_2 = 30$ nm, $L_1 = 340$ nm, and $L_2 = 270$ nm. The length of the middle rod is 260 nm. The periods in both the x and y directions are 700 nm. The in-plane distance between the two rods in each rod pair is 150 nm. (**C**) Level scheme for two quadrupolar resonances that are coupled to a dipole in a schematic four-level system. Resonance I (see Fig. 2B) results from destructive interference between pathways |0> –|1> and |0> – |1> –|2> –|1>. Resonance II (see Fig. 2B) results from destructive interference between pathways |0> –|1> and |0> –|1> –|3> –|1>.

electron microscopy (SEM). An overview of a typical sample is shown in Fig. 1B. The near-infrared transmittance, reflectance, and absorbance spectra of the samples at normal incidence were measured by a Fourier-transform infrared spectrometer with electric field polarization parallel to the middle red rod.

The optical properties of the 3D ruler can be understood by first starting with the highest-symmetry configuration (the bottom curve in Fig. 2A), in which the yellow and green rod pairs are of equal length ($\Delta L = L_1 - L_2 = 0$ nm), and the central dipole-coupled red rod sits along the symmetry axis of the two quadrupole-coupled rod pairs ($S = 0$ nm). In this case, there is only a single broad resonance visible from the excitation of the dipolar plasmons in the single nanorod (*10*). Excitation of the quadrupolar modes can occur only when the system symmetry is reduced, giving rise to near-field coupling between the dipolar and quadrupolar resonances. For example, when a displacement of the middle rod is introduced ($S = 40$ nm), a transparency window appears inside the broad outer resonance profile (middle curve in Fig. 2A). By introducing a length difference between the two rod pairs ($\Delta L = L_1 - L_2 = 70$ nm) while keeping the displacement at $S = 40$ nm, a dip in the transmittance emerges in the middle of the transparency window, giving rise to two transmittance peaks (top curve in Fig. 2A). Simulations for the optical spectra were performed based on a finite integration time domain algorithm as well as the Fourier modal method (*15*). The permittivity of the gold is described by the Drude model (*16*). The plasma frequency is $\omega_{pl} = 1.37 \times 10^{16}$ s^{-1}. Owing to the surface scattering and grain boundary effects in the thin film, the simulation results are obtained using a higher damping constant than the bulk value, $\omega_c = 1.22 \times 10^{14}$ s^{-1} (*14*). The refractive indices of the glass substrate and PC403 are taken as 1.5 and 1.55, respectively. Figure 2B presents the calculated transmittance spectra of the samples. The experimental results show an excellent overall agreement with the numerical predictions. The corresponding reflectance and absorbance spectra are presented in fig. S2 (*17*). Calculated current distributions at the respective spectral positions I and II as indicated in Fig. 2B are displayed below the spectra in Fig. 2. In particular, a quadrupolar current distribution in the longer top rod pair is observed at the spectral position of transmittance peak I, and likewise a quadrupolar current distribution in the bottom shorter rod pair is visible at the spectral position of transmittance peak II.

Figure 1C shows a schematic four-level system (*18*, *19*), which can be used to interpret the above phenomena. In our structure, the red middle rod is strongly coupled to light, giving rise to a broad dipolar (bright) resonance due to radiative losses. This can be correlated with the dipole-allowed transition from |0> to |1>. The green and yellow rod pairs can support quadrupolar modes, which are subradiant (dark). They can be correlated with the two dipole-forbidden transitions from |0> to |2> and |0> to |3>, respectively. These two quadrupolar modes are associated with very narrow resonances, whose linewidths are solely determined by the nonradiative damping in the metal. In the presence of a nonzero displacement S, the two dark quadrupoles can be strongly coupled to the middle dipole by near-field coupling. As a result, destructive interference of two excitation pathways, namely the direct excitation of the dipolar mode in the red rod (|0> – |1>) and the indirect excitation due to its interactions with the quadrupolar modes in the yellow (|0> – |1> – |2> – |1>) and green (|0> – |1> – |3> – |1>) rod pairs, results in transmittance peaks at resonances I and II, respectively. Consequently, due to this destructive interference, currents are nearly absent in the middle rod at these two resonances. This is evident from the current distributions in Fig. 2. The middle curve in Fig. 2A is correlated with the degenerate case, where the two quadrupoles have approximately identical resonance energies (*20*). A more extensive structural tuning to optimize the double quadrupolar resonances is shown in fig. S1 (*17*).

The key elements of the use of our structure as a 3D plasmon ruler are the sharp spectral features of the quadrupolar resonances and their extremely high sensitivity to any spatial or structural changes. The dipolar resonance profile, which is generally used for detecting spectral shifts in plasmon rulers, is divided by two quadrupolar resonances that lead to significantly reduced linewidths and therefore increased figures of merit. This is a fundamental criterion for the implementation of sensitive plasmon rulers. In the near-field regime, dipole-quadrupole coupling is more distance-dependent than dipole-dipole coupling. The use of the 3D plasmonic structure allows us to retrieve 3D structural changes that occur owing to the transition from one configuration to another by reading out spectral changes of the well-modulated plasmon spectra.

A minute conformational change of the 3D plasmonic structure can give rise to an appreciable variation of the optical spectra. We start with the structural configuration ($\Delta L = L_1 - L_2 = 70$ nm)

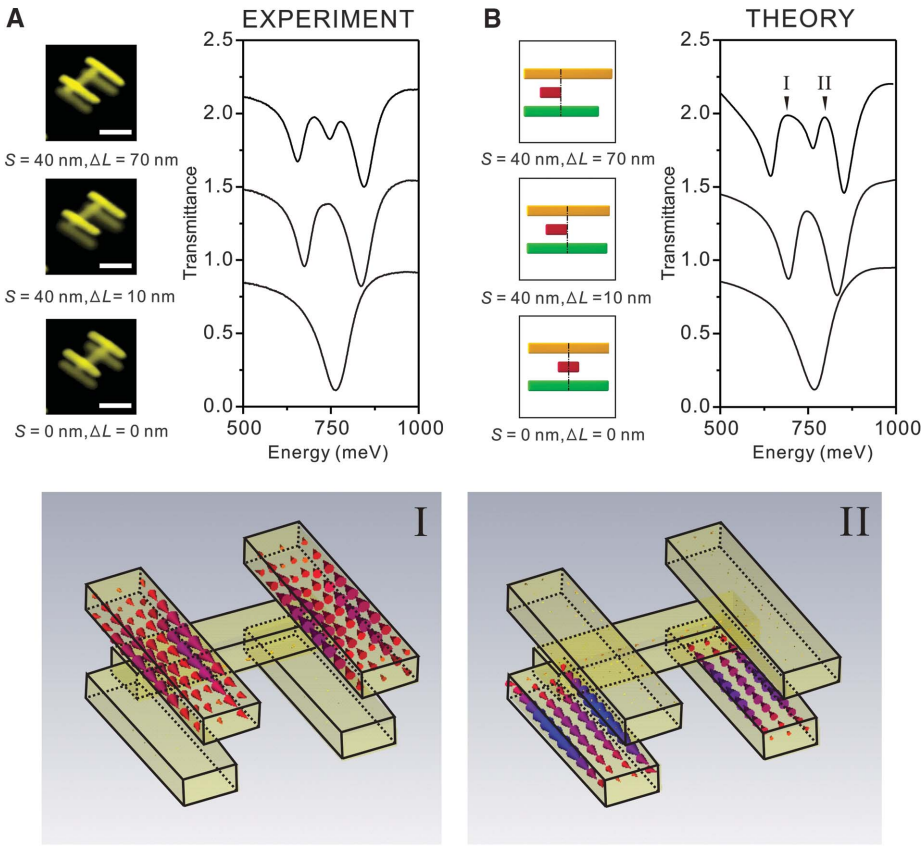

Fig. 2. (**A**) Experimental and (**B**) calculated transmittance spectra of the 3D plasmon ruler in dependence on structural tuning. Spectra are shifted upward for clarity. Bottom curves: $S = 0$ nm, $L_1 = 310$ nm, and $L_2 = 310$ nm ($\Delta L = L_1 - L_2 = 0$ nm). Middle curves: $S = 40$ nm, $L_1 = 310$ nm, and $L_2 = 300$ nm ($\Delta L = 10$ nm). Top curves: $S = 40$ nm, $L_1 = 340$ nm, and $L_2 = 270$ nm ($\Delta L = 70$ nm). The SEM images of the nanostructures are shown in (A) accordingly. One and two transmittance peaks develop inside the broad dipolar absorption dip, depending on the degree of structural symmetry breaking. (Bottom) Calculated current distributions at resonances I and II. At resonance I, antisymmetric charge oscillations are excited in the top rod pair, and at resonance II, they are excited in the bottom rod pair; in both cases, the middle rod contains almost no current.

of Fig. 2A. Figure 3A shows the experimental spectra, in which the lateral displacement S is successively decreased from 40 to 0 nm. The calculated spectra (Fig. 3B) show an excellent agreement with the experimental results. The corresponding reflectance and absorbance spectra are to be found in fig. S3 (*17*). Examining the intensities of the resonances (which were extracted from the experimental transmittance spectra), one can gain further insight into the relation between the spatial structural changes and the optical response (Fig. 4A). As S decreases, the two quadrupolar resonances are both suppressed because of the reduced structural asymmetry. The higher-energy quadrupolar resonance (resonance II) subsides much faster than the lower-energy one (resonance I). This is due to the fact that resonance II is associated with the bottom shorter rod pair. A slight lateral detuning of the middle rod has a larger influence on this shorter rod pair than on the top longer rod pair because of the asymmetric structural configuration (see the schematic in Fig. 3A). Subsequently, resonance II vanishes when the single middle rod is placed overlapping with the symmetry axis of the bottom shorter rod pair (i.e., $S = 0$ nm). In this case, resonance I is still visible because the middle rod has a finite displacement with respect to the symmetry axis of the longer rod pair. In essence, a minute spatial change within the 3D plasmonic structure can give rise to distinct shape and intensity variations in the optical spectra. The 3D plasmon ruler is not solely based on the colorimetric detection scheme but rather on the full well-modulated plasmonic spectral behavior.

Taking this concept a step further, we show that the spatial degrees of freedom of the 3D plasmonic structure allow for distinguishing the direction as well as the magnitude of the structural change. Calculations were performed on our 3D plasmonic structure with the middle rod vertically displaced. The calculated transmittance spectra are shown in Fig. 3B. When the middle rod is vertically shifted upward or downward from the middle position of the two rod pairs, it leads to distinctly detuned resonance profiles of the two quadrupolar modes. Figure 4B shows the calculated intensities of the two quadrupolar res-

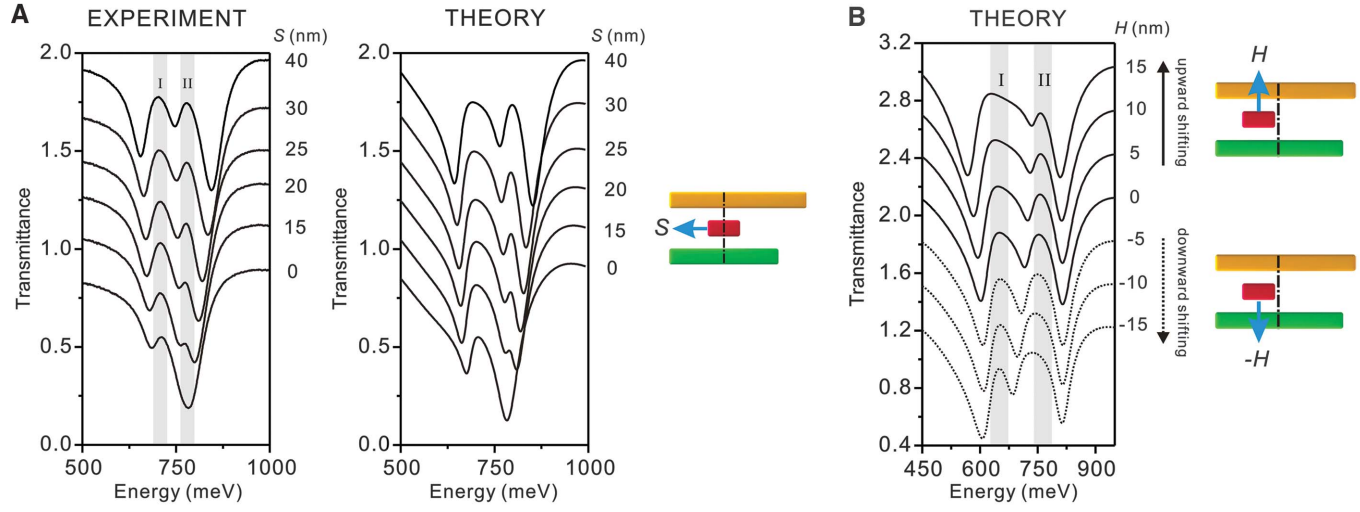

Fig. 3. (**A**) Experimental (left) and calculated (right) transmittance spectra of the 3D plasmon ruler in dependence on lateral displacement S. Spectra are shifted upward for clarity. The geometrical parameters are $L_1 = 340$ nm and $L_2 = 270$ nm. The length of the middle rod is 260 nm. The weight of the two quadrupolar transmittance peaks is strongly dependent on the lateral displacement of the dipolar rod. (**B**) Calculated spectra of the 3D plasmon ruler in dependence on vertical displacement H. Spectra are shifted upward for clarity. The geometrical parameters are $S = 50$ nm, $L_1 = 360$ nm, and $L_2 = 290$ nm. The length of the middle rod is 290 nm. The middle rod is shifted successively upward or downward in steps of 5 nm. The intensity, width, and spectral position of the quadrupolar transmittance peaks depend sensitively on the vertical displacement of the dipolar rod.

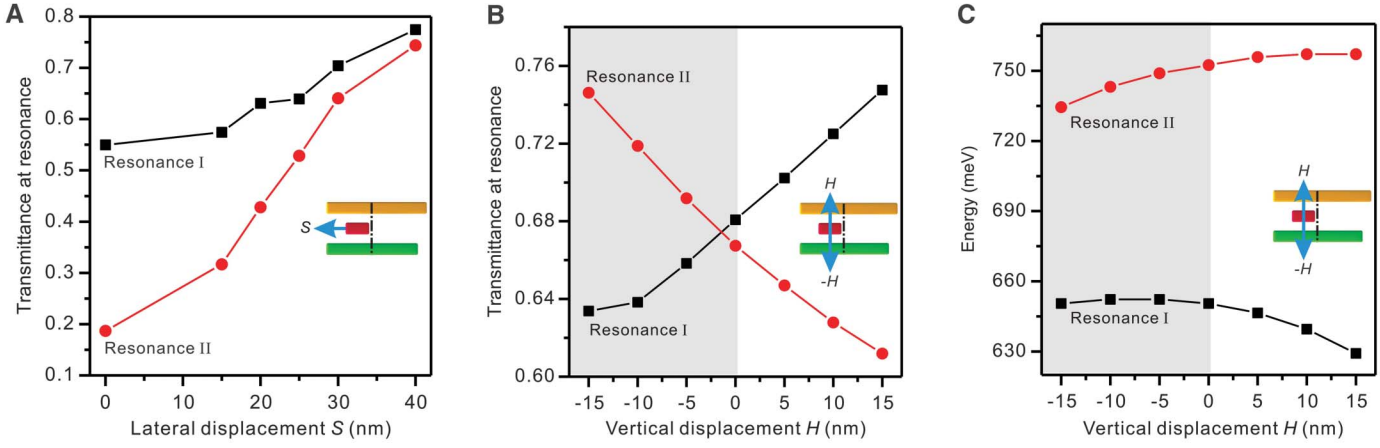

Fig. 4. (**A**) Transmittance intensities of the two quadrupolar resonances in dependence on lateral displacement S, which are extracted from the experimental transmittance spectra in Fig. 3A. When S is successively decreased, both quadrupolar resonances become smaller. Resonance II diminishes much faster than resonance I. (**B**) Transmittance intensities of the two quadrupolar resonances in dependence on H, which are extracted from the transmittance spectra in Fig. 3B. The two resonance branches show opposite distance dependence and cross one another. (**C**) Spectral positions of the two quadrupolar resonances in dependence on H, which are extracted from the transmittance spectra in Fig. 3B. Resonances I and II exchange their distance-dependence behavior in $H > 0$ (white) and $H < 0$ (gray) areas. The sensitive behavior of the spectral features allows for extraction of the 3D structural changes.

onances in dependence on *H*. When *H* decreases, resonances I and II show opposite spectral behavior, and the transmittance intensities of the two resonance branches cross one another. In particular, resonance I evolves from a broad profile to a narrower and suppressed resonance, whereas resonance II grows in strength and becomes more and more pronounced. This is due to the fact that when the middle rod is successively shifted toward the bottom shorter rod pair and therefore couples more strongly to it, resonance II is enhanced. Simultaneously, resonance I is reduced because the middle rod is shifted gradually away from the top longer rod pair and therefore couples less strongly to it. It is noteworthy that the spectral positions of the two quadrupolar resonances can also provide information on the spatial structure change. Figure 4C shows the calculated spectral positions of the two quadrupolar resonances in dependence of *H*. When the middle rod is shifted downward (see the gray region), the position of resonance I stays nearly the same, whereas resonance II shifts to lower energies. In contrast, when the middle rod is shifted upward (see the white region), resonance II does not show a prominent position change, whereas resonance I shifts to significantly lower energies. Figure 4 clearly demonstrates how the full spectral behavior of the 3D plasmonic structure is correlated to the structural changes in space and will allow for evaluation of the magnitudes as well as the directions of structural changes. Differential spectra that evaluate 3D conformational changes from the initial configuration to successive configurations offer even more distinct spectral features and facilitate the identification of specific motions. Figures S4 and S5 (*17*) show how this can aid the spectral analysis of the 3D ruler system upon minute structural tilting and twisting.

To demonstrate the fundamental concepts of 3D plasmon rulers, we used in our study a complex sequence of nanolithography steps. The resulting optical response of the 3D plasmon ruler has been correlated with the particle plasmon resonances of the individual nanostructure assembly. The same concepts can be applied to single metallic nanocrystals joined together by oligonucleotides or peptides (*21*–*24*), giving rise to a new generation of plasmon rulers with unprecedented ability to monitor the sequence of events that occur during a wide variety of macromolecular transformations in three dimensions. Metallic nanoparticles of different lengths or sizes could be attached at different positions of the DNA or protein (*25*, *26*), and each metallic element may move individually or collectively in three dimensions. Dark-field microspectroscopy of the scattering or the extinction spectrum would offer a useful tool to identify the 3D arrangement of the different constituents in real time, as it is unambiguously correlated to very distinct and rich spectral features. As in the case of nuclear magnetic resonance, 3D plasmon rulers could use a lookup database where the optical spectra corresponding to all possible structural configurations are stored. Spectral features can then be associated with certain distortions. Novel methods of data mining and inference would facilitate this task. This concept can be further extended by using polarization sensitivity as well as tomography-like spectroscopy from different directions. The realization of 3D plasmon rulers using nanoparticles and biochemical linkers is challenging, but 3D nanoparticle assemblies with desired symmetries and configurations have been successfully demonstrated very recently (*24*, *25*, *27*–*30*). These exciting experimental achievements will pave the road toward the realization of 3D plasmon rulers in biological and soft-matter systems.

References and Notes

1. C. Sönnichsen, B. M. Reinhard, J. Liphardt, A. P. Alivisatos, *Nat. Biotechnol.* **23**, 741 (2005).
2. G. L. Liu *et al.*, *Nat. Nanotechnol.* **1**, 47 (2006).
3. Y. W. Jun *et al.*, *Proc. Natl. Acad. Sci. U.S.A.* **106**, 17735 (2009).
4. L. Stryer, *Annu. Rev. Biochem.* **47**, 819 (1978).
5. J. A. Fan *et al.*, *Science* **328**, 1135 (2010).
6. M. Hentschel *et al.*, *Nano Lett.* **10**, 2721 (2010).
7. J. B. Lassiter *et al.*, *Nano Lett.* **10**, 3184 (2010).
8. C. Sönnichsen, A. P. Alivisatos, *Nano Lett.* **5**, 301 (2005).
9. S. Zhang, D. A. Genov, Y. Wang, M. Liu, X. Zhang, *Phys. Rev. Lett.* **101**, 047401 (2008).
10. N. Liu *et al.*, *Nat. Mater.* **8**, 758 (2009).
11. N. Liu *et al.*, *Nano Lett.* **10**, 1103 (2010).
12. N. Papasimakis, V. A. Fedotov, N. I. Zheludev, S. L. Prosvirnin, *Phys. Rev. Lett.* **101**, 253903 (2008).
13. P. Tassin, L. Zhang, T. Koschny, E. N. Economou, C. M. Soukoulis, *Phys. Rev. Lett.* **102**, 053901 (2009).
14. N. Liu *et al.*, *Nat. Mater.* **7**, 31 (2008).
15. G. Granet, J. P. Plumey, *J. Opt. A* **4**, S145 (2002).
16. M. A. Ordal *et al.*, *Appl. Opt.* **22**, 1099 (1983).
17. See supporting material on *Science* Online.
18. C. L. G. Alzar, M. A. G. Martinez, P. Nussenzveig, *Am. J. Phys.* **70**, 37 (2002).
19. M. Fleischhauer, A. Imamoglu, J. P. Marangos, *Rev. Mod. Phys.* **77**, 633 (2005).
20. H. Xu, Y. Lu, Y. Lee, B. S. Ham, *Opt. Express* **18**, 17736 (2010).
21. C. D. Mao, W. Q. Sun, N. C. Seeman, *Nature* **386**, 137 (1997).
22. E. Winfree, F. R. Liu, L. A. Wenzler, N. C. Seeman, *Nature* **394**, 539 (1998).
23. J. P. Zheng *et al.*, *Nature* **461**, 74 (2009).
24. S. J. Tan, M. J. Campolongo, D. Luo, W. Cheng, *Nature Nanotechnol.*, 10.1038/nnano.2011.49 (2011).
25. A. J. Mastroianni, S. A. Claridge, A. P. Alivisatos, *J. Am. Chem. Soc.* **131**, 8455 (2009).
26. J. Sharma *et al.*, *Science* **323**, 112 (2009).
27. P. Cigler, A. K. R. Lytton-Jean, D. G. Anderson, M. G. Finn, S. Y. Park, *Nat. Mater.* **9**, 918 (2010).
28. M. R. Jones *et al.*, *Nat. Mater.* **9**, 913 (2010).
29. J. W. Zheng *et al.*, *Nano Lett.* **6**, 1502 (2006).
30. D. R. Han *et al.*, *Science* **332**, 342 (2011).

Acknowledgments: We thank T. Pfau and M. Dressel for useful discussions and comments and S. Hein for his material visualizations. N.L. and A.P.A. were supported by the NIH Plasmon Rulers Project, grant NIH NOT-OD-09-056. M.H., T.W., and H.G. were financially supported by the Deutsche Forschungsgemeinschaft (DFG) (grants SPP1391 and FOR557), by The German Ministry of Science (grants 13N9048 and 13N10146), and by Landesstiftung B. W.T.W. were also supported by the DFG (grant GI 269/11-1) and by Deutsch-Französische Hochschule–Université franco-allemande.

Supporting Online Material

www.sciencemag.org/cgi/content/full/332/6036/1407/DC1
Materials and Methods
Figs. S1 to S5

3 November 2010; accepted 12 May 2011
10.1126/science.1199958

Direct Observation of Nodes and Twofold Symmetry in FeSe Superconductor

Can-Li Song,[1,2] Yi-Lin Wang,[2] Peng Cheng,[1] Ye-Ping Jiang,[1,2] Wei Li,[1] Tong Zhang,[1,2] Zhi Li,[2] Ke He,[2] Lili Wang,[2] Jin-Feng Jia,[1] Hsiang-Hsuan Hung,[3] Congjun Wu,[3] Xucun Ma,[2]* Xi Chen,[1]* Qi-Kun Xue[1,2]

We investigated the electron-pairing mechanism in an iron-based superconductor, iron selenide (FeSe), using scanning tunneling microscopy and spectroscopy. Tunneling conductance spectra of stoichiometric FeSe crystalline films in their superconducting state revealed evidence for a gap function with nodal lines. Electron pairing with twofold symmetry was demonstrated by direct imaging of quasiparticle excitations in the vicinity of magnetic vortex cores, Fe adatoms, and Se vacancies. The twofold pairing symmetry was further supported by the observation of striped electronic nanostructures in the slightly Se-doped samples. The anisotropy can be explained in terms of the orbital-dependent reconstruction of electronic structure in FeSe.

Despite intense experimental investigation, the pairing symmetry in the recently discovered iron (Fe)–based superconductors remains elusive (*1*–*3*). Phonon-mediated pairing in conventional superconductors is typically isotropic, leading to *s*-wave symmetry. Unconventional pairing mechanisms, such as spin fluctuations, may give rise to an order parameter with its sign change over the Fermi surfaces and a pairing symmetry such as $s\pm$ (*4*, *5*). The $s\pm$ scenario is supported by the phase-sensitive "Josephson tunneling" (*6*, *7*) and angle-resolved photoemission spectroscopy (*8*) experiments. If the sign change occurs on a single electron or

[1]State Key Laboratory for Low-Dimensional Quantum Physics, Department of Physics, Tsinghua University, Beijing 100084, the People's Republic of China. [2]Institute of Physics, Chinese Academy of Sciences, Beijing 100190, the People's Republic of China. [3]Department of Physics, University of California, San Diego, La Jolla, CA 92093–0319, USA.

*To whom correspondence should be addressed. E-mail: xcma@aphy.iphy.ac.cn (X.M.); xc@mail.tsinghua.edu.cn (X.C.)